Analytical Biochemistry 602 (2020) 113798

Contents lists available at ScienceDirect

Analytical Biochemistry

journal homepage: www.elsevier.com/locate/yabio

Colorimetric biosensing of nopaline synthase terminator using Fe_3O_4@Au and hemin-functionalized reduced graphene oxide

Xiaodong Cao[a], Zihao Xia[a], Wuwen Yan[a], Shudong He[a], Xuan Xu[b], Zhaojun Wei[a], Yongkang Ye[a,*], Haisong Zheng[c]

[a] School of Food Science and Biological Engineering, Hefei University of Technology, Hefei, 230009, China
[b] College of Chemistry and Molecular Engineering, Nanjing Tech University, Nanjing, 211816, China
[c] Technology Center of Hefei Customs, Hefei, 230032, China

ARTICLE INFO

Keywords:
Colorimetric biosensor
Label-free
Genetically modified (GM) plants
Peroxidase-mimicking activity

ABSTRACT

In this paper, we present a simple and label-free colorimetric biosensor for detection of the nopaline synthase (NOS) terminator in genetically modified (GM) plants. The "signal on" colorimetric biosensor was developed using a nanocomposite consisted of gold nanoparticles doped magnetic Fe_3O_4 nanoparticles (Fe_3O_4@Au NP), capture probe DNA (cDNA), and hemin-functionalized reduced graphene oxide nanosheets (H-GN). The nanocomposite was successfully prepared by means of Au–S bonds and the strong π interactions between cDNA and H-GN. The sensing approach is based on the excellent peroxidase-mimicking activity of H-GN and its different electrostatic interactions with single-stranded DNA (ssDNA) and double-stranded DNA (dsDNA). In presence of the target NOS, the cDNA in the nanocomposite will hybridize with its complementary sequence, and form dsDNA structure. Due to the weak π interactions between dsDNA and H-GN, a portion of H-GN will be released from the surface of Fe_3O_4@Au NPs and transferred into solution. After magnetic separation was performed, the supernatant was incubated with 3,3′,5,5′-tetramethylbenzidine (TMB) in the presence of H_2O_2. The released H-GN can catalyze the oxidation reaction of TMB and turn the colorless solution blue. This "signal-on" colorimetric biosensor shows a broad linear range of 0.5–100 nM for the target NOS, with a 0.19 nM detection limit. The application of the biosensor for determination of NOS segments in samples of GM and non-GM tomatoes shows that it can discriminate between GM and non-GM plants. The reliability of the method for samples of NOS-spiked GM tomato suggests satisfactory recoveries in the range of 93.6%–94.2%.

1. Introduction

According to the report issued in 2018 by International Service for the Acquisition of Agri-biotech Applications (ISAAA), genetically modified (GM) crops have been grown in 26 countries with total planting area of 191.7 million hectares. Seventy countries have approved the use of GM crops in food, feed and processing [1]. Meanwhile, the debate about the potential risks on ecosystem and human health caused by the cultivation of GM plants and the consuming GM food products has never stopped [2,3]. Required for the safety of ecosystems and guaranteed information for consumers, an increasing number of countries have made legislation regarding the thresholds for GM planting and GM food labeling. Therefore, there is an urgent need to develop reliable and cost-effective analytical methods for GM screening [4,5].

Analytical methods for identification of GM content rely on either protein or DNA detection [6–8]. DNA-based methods have been more frequently chosen for the detection of GM contents in GM crops or foods [9]. As Cauliflower Mosaic Virus 35S (CaMV35S) promoter and nopaline synthase (NOS) terminator are the most commonly used DNA elements in regulating expression in GM crops [4,5], they are often selected for screen GM crops. Currently, the conventional and recommended method for GM contents determination is still based on the amplification of target DNA sequences using polymerase chain reaction (PCR) [10,11]. However, PCR-based assays still have some shortcomings such as being time-consuming and costly. Many researchers have devoted efforts to improving PCR-based assays to shorten the PCR reaction [5,12–14]. Regardless, an increasing number of researchers are focusing on developing alternative methods for detection of GM contents [3,7,8,15]. Colorimetric assays for the detection of DNA are simple, rapid and affordable. Most importantly, the color change can be discerned by the naked eyes. In this sense, the colorimetric method

* Corresponding author.
E-mail address: yongkang.ye@hfut.edu.cn (Y. Ye).

https://doi.org/10.1016/j.ab.2020.113798
Received 16 March 2020; Received in revised form 23 May 2020; Accepted 25 May 2020
Available online 04 June 2020
0003-2697/

seems to be a suitable and promising way to determine and screen GM content in GM crops or GM food products [16–18].

Improving the sensitivity is a crucial issue for all biosensors, and colorimetric biosensors are no exception. Several strategies have been investigated and used to enhance the sensitivity of colorimetric biosensors. One of these strategies is to amplify the target genes using loop-mediated isothermal amplification (LAMP) [15,19,20]. For example, a colorimetric method was developed for CaMV35S determination using the LAMP method with acid chrome blue K (ACBK) as a novel metal indicator [19]. During the LAMP reaction, the color of the solution changed from red to blue. Such change was easy to be judged by the naked eyes. This novel colorimetric biosensor gave a sensitivity threshold of approximately 50 copies for transgenic rice genomic DNA. Another strategy that commonly adopted is to apply nanomaterials in the constructing of colorimetric biosensors. Various nanomaterials that possess peroxidase-like activity have gained popularity in the chromogenic reaction system of 3,3′,5,5′-tetramethylbenzidine (TMB) and H_2O_2. These nanomaterials include metal nanoclusters [21,22] and nanoparticles [23], metal oxide nanoparticles [24,25], and carbon nanomaterials [26–28]. In recent years, graphene-based nanosheets that exhibit excellent peroxidase-like activity have been widely applied in DNA determination [27,28]. For instance, Tao et al. synthesized hemin, a chemical with mimicking peroxidase activity, functionalized graphene (H-GN), and exploited it as a platform for colorimetric assays for DNA sensing [28]. By utilizing the strong affinity between single strand DNA (ssDNA) sequences and graphene, the authors separately prepared probe DNA1 (59 bp) and DNA2 (59 bp) biofunctionalized H-GN (DNA1-H-GN and DNA2-H-GN, respectively). Both DNA1 and DNA2 had a target-specific sequence complementary to target DNA (tDNA, 27 bp) at the 5′/3′ terminus. After adding tDNA into the mixture of DNA1-H-GN and DNA2-H-GN, sandwich-type DNA-GH hybrids were formed through DNA hybridization. After centrifugation, the supernatant containing fewer DNA1-H-GN and DNA2-H-GN was collected and incubated with TMB and H_2O_2. The colorimetric signal of the chromogenic reaction system decreased with the decreasing amount of DNA1-H-GN and DNA2-H-GN. Thus, a “signal-off” biosensor with a detection limit of 0.5 nM was successfully prepared.

Noble metal-functionalized magnetic nanoparticles have been widely used in construction of biosensors due to their good magnetism, ease of preparation and surface modification, and good biocompatibility [8,29,30]. Wang et al. synthesized gold nanoparticles (Au NP)-doped Fe_3O_4 magnetic nanoparticles (Fe_3O_4@Au MNP). By taking advantage of its peroxidase-like activity and superparamagnetism, this material has been used as signal indicator and magnetic separator for colorimetric aptasensing of ochratoxin A [29]. Herein, fascinated by the excellent peroxidase-mimicking activity of H-GN and the good properties of Fe_3O_4@Au MNP, we developed a “signal-on” genosensor for label-free colorimetric determination of NOS terminator gene sequences. As shown in Scheme 1, we first prepared Fe_3O_4@Au MNPs according to our previous work [8] first. After biofunctionalizing the surface of Fe_3O_4@Au NPs with capture DNA (cDNA) via Au–S bonds, the resulting material was used to form Fe_3O_4@Au@cDNA@H-GN nanocomposite by making use of the strong affinity between ssDNA and H-GN. In the presence of tDNA, cDNA in the Fe_3O_4@Au@cDNA@H-GN nanocomposite can hybridize with tDNA and then form double-helix structures. Such an event will release a portion of H-GN from the surface of the Fe_3O_4@Au MNPs due to the weak affinity between double-strand DNA (dsDNA) and H-GN. The greater the amount of tDNA that was added, the greater the amount of H-GN that was released. After magnetic separation, the supernatant was collected and incubated in TMB and H_2O_2. The released H-GN exhibited its peroxidase-mimicking activity in the oxidation reaction of TMB and then turned the colorless solution blue. The intensity of the color depended on the amount of the released H-GN. Based on this approach, a “signal-on” colorimetric genosensor for label-free determination of the target NOS was developed.

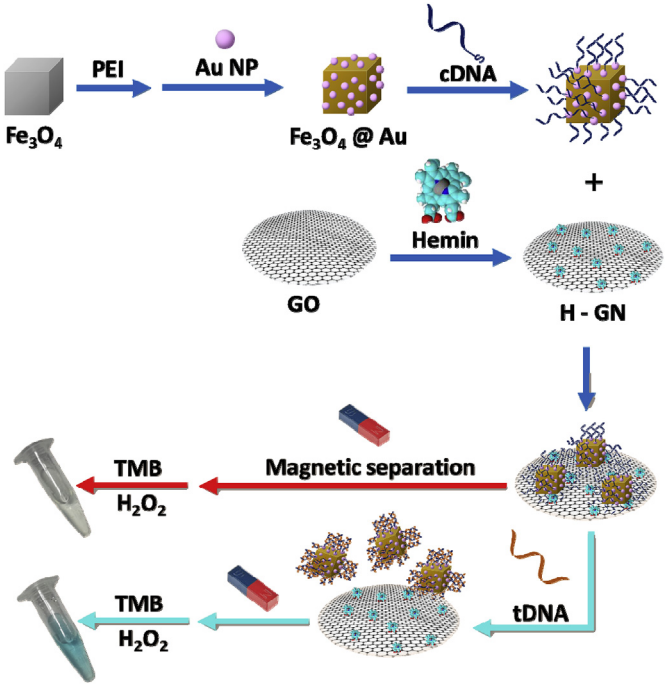

Scheme 1. The strategy for determination of target NOS sequences.

2. Materials and methods

2.1. Reagents

Graphene oxide was supplied by Nanjing XF Nano Co., Ltd. (Nanjing, China). Chloroauric acid ($HAuCl_4{\cdot}4H_2O$), sodium borohydride ($NaBH_4$), ethylenediamine tetraacetic acid (EDTA), hydrazine hydrate ($N_2H_4{\cdot}H_2O$) and H_2O_2 were obtained from National Medicine Group Shanghai Chemical Reagent Co., Ltd. (Shanghai, China). Hemin, polyethyleneimine (PEI), TMB and Tris-(2-carboxyethyl) phosphine (TCEP) were purchased from Aladdin Industrial Co., Ltd. (Shanghai, China). The buffer solutions used in the present work are as follows, DNA stock buffer/TE buffer: pH 7.4, 10 mM Tris-HCl, 1.0 mM EDTA; DNA immobilization buffer: pH 7.4, 10 mM Tris-HCl, 1.0 mM EDTA, 1.0 mM TCEP, 100 mM NaCl, 1.0 mM $MgCl_2$; hybridization buffer solution: 10 mM Tris-HCl, 1.0 mM EDTA, 100 mM NaCl, and 1.0 mM $MgCl_2$; colorimetric reaction solution: pH 5.0, 25 mM phosphate buffer solution; and CTAB buffer: pH 8.0, 100 mM Tris-HCl, 20 mM EDTA, 1.4 M NaCl, 2% CTAB. Ultrapure water was used throughout the experiment.

All DNA sequences were synthesized and purified by Shanghai Sangon Biotechnology Co., Ltd. (Shanghai, China), and their sequences are as follows:

Capture sequences (cDNA): 5′-SH-T CTC TCA TAA ATA ACG TCA TGC-3’;
NOS sequences (tDNA): 5′-GCA TGA CGT TAT TTA TGA GAG A-3’;
single-base mismatched DNA (Mis-1): 5′-GCA TGA CGT T***G***T TTA TGA GAG A-3′;
double-base mismatched DNA (Mis-2): 5′-GCA TGA C***T***T T***G***T TTA TGA GAG A-3′;
three-base mismatched DNA (Mis-3): 5′-GCA TGA C***T***T T***G***T TTA T***A***A GAG A-3′; and
CaMV35S sequences: 5′-ATT GTG CGT CAT CCC TTA CGT C-3′.

2.2. Apparatus

UV–vis absorption spectra were recorded on a UV-4802

spectrophotometer (Unico Shanghai Instrument Co., Ltd. Shanghai, China). X-ray photoelectron spectroscopy (XPS) analysis was performed on an ESCALAB250 X-ray photoelectron spectrometer (Thermo Fisher Scientific, USA) using Al Kα (1486.6 eV) radiation at a power of 225 W. Field emission scanning electron microscopy (SEM) and transmission electron microscopy (TEM) were performed on SU8020 (Hitachi, Japan) and JEM-1400 flash (JEOL, Japan) system, respectively. PCR amplification was carried out on a TC-96/T/H system (Hangzhou Bioer Technology Co., Ltd. Hangzhou, China).

2.3. Synthesis of H-GN

H-GN was synthesized according to our previous work [31] with minor modifications. Briefly, 20 mL of 0.5 mg mL^{-1} hemin was mixed with 20 mL of 0.5 mg mL^{-1} GO solution under vigorous stirring in a flask. Then, 200 μL of aqueous ammonia solution (28%) and 30 μL of hydrazine hydrate solution (25%) were added into the above mixture. After 3 min of vigorous stirring, the flask was placed in a water bath at 60 °C, and the reaction lasted for 24 h. The black suspension was cooled to room temperature, followed by centrifugation and washing with water several times. The prepared H-GN was collected and redispersed in water for later use. At the same time, chemically reduced graphene (rGO) nanosheets were prepared using the same method for comparison.

2.4. Synthesis of Fe_3O_4 and Fe_3O_4@Au MNP

Fe_3O_4 MNPs were synthesized using coprecipitation method [32]. Typically, $FeCl_3{\cdot}6H_2O$ (16.22 g) and $FeCl_2{\cdot}4H_2O$ (5.95 g) were dissolved in a mixture of 1 mL of 80% (v/v) hydrazine hydrate (25%) and 300 mL of deoxygenated ultrapure water. The above mixture was stirred under a nitrogen atmosphere until $FeCl_3{\cdot}6H_2O$ and $FeCl_2{\cdot}4H_2O$ were fully dissolved. Then, 60 mL of ammonia solution (28%) was added dropwise at 60 °C. The reaction proceeded for 90 min. Next, the obtained suspension was allowed to cool to room temperature. The synthesized Fe_3O_4 MNPs were washed several times with water. Finally, these nanoparticles were dried under vacuum at 50 °C for 24 h.

Spherical Au NPs with an average diameter of 4 nm were prepared according to a literature protocol [8,33]. Subsequently, the Fe_3O_4@Au MNPs were prepared in two steps [8]. First, 50 mg of the prepared Fe_3O_4 magnetic nanoparticles were dispersed in 12.5 mL of PEI (0.8%) solution using ultrasonication. One hour later, the PEI-wrapped Fe_3O_4 nanoparticles were separated from the solution and washed several times with water. Second, the PEI-wrapped Fe_3O_4 MNPs were mixed with the Au NP solution (7 mL) and left ultrasonicating for 1 h. The product was washed, magnetically collected and dried at 50 °C to obtain Fe_3O_4@Au MNPs.

2.5. Synthesis of Fe_3O_4@Au@cDNA@H-GN nanocomposite

To prepare Fe_3O_4@Au@cDNA@H-GN, cDNA biofunctionalized Fe_3O_4@Au (Fe_3O_4@Au@cDNA) was first prepared. Briefly, 2.5 mg of Fe_3O_4@Au was dispersed in 5 mL of DNA immobilization buffer, followed by the addition 500 μL of 10 μM thiolated cDNA. The reaction lasted for 24 h at 4 °C with constant shaking. Subsequently, Fe_3O_4@Au@cDNA was magnetically separated and thoroughly washed several times to remove the unbound cDNA. The obtained Fe_3O_4@Au@cDNA was then dispersed in 1 mL of TE buffer.

The Fe_3O_4@Au@cDNA@H-GN nanocomposite was prepared by mixing 25 mL of H-GN (0.5 mg mL^{-1}) with 1 mL of Fe_3O_4@Au@cDNA. The suspension was gently shaken for 12 h. The prepared Fe_3O_4@Au@cDNA@H-GN was then collected with a magnet and washed several times to remove the unattached H-GN. The resultant Fe_3O_4@Au@cDNA@H-GN nanocomposite was finally suspended in 5 mL of TE buffer and stored at 4 °C for later use.

2.6. Preparation of real samples and PCR product of the NOS gene sequences

The target NOS gene segments in real samples were extracted from laboratory-grown transgenic tomatoes using the CTAB method [34]. The leaves of GM tomato (1 g) were ground with liquid nitrogen first, followed by incubation in CTAB buffer (600 μL) at 65 °C for 1 h with occasional stirring. The mixture was then cooled to room temperature. Next, chloroform (700 μL) was added, and the mixture was shaken for 3 min. After centrifugations at 1000 rpm for 10 min, the supernatant was mixed with isopropanol (400 μL) and incubated for 30 min at −20 °C. The mixture was subsequently centrifuged at 12,000 rpm for 10 min at 4 °C. Then the precipitate was collected and washed with ethanol (75%) several times. The obtained pellet was dried at room temperature and finally dissolved in water and stored at −20 °C until use.

The PCR was carried out in a reaction system with a total solution volume of 50 μL containing 5 μL of 10 × PCR buffer, 5 μL of the extracted DNA, 1 μL of forward and reverse primers (10 μM), 1 μL of Taq DNA polymerase (5 U μL^{-1}), 1 μL of dNTP (10 mM), 3 μL $MgCl_2$ (25 mM) and 33 μL water. The amplification was conducted as follows: denaturation at 94 °C for 5 min, and then running 30 cycles of amplification at 94 °C for 30 s, annealing at 57 °C for 30 s, extension at 72 °C for 30 s, and final extension at 72 °C for 4 min. The PCR product was determined by running 10 μL of the PCR mixture in a 1% agarose gel for 20 min. The electrophoretic bands were observed under ultraviolet light.

2.7. Colorimetric detection of NOS gene sequences

Before hybridization, the suspension of Fe_3O_4@Au@cDNA@H-GN was thoroughly blended with a vortex mixer. The hybridization reaction was conducted by mixing 50 μL of Fe_3O_4@Au@cDNA@H-GN with 10 μL of the target NOS solution. The reaction was performed at 37 °C for 2 h under gentle shaking. The supernatant was afterwards separated from solid particles with a magnet. Next, the collected supernatant was mixed thoroughly with 1 mL of 25 mM phosphate buffer solution contained 0.4 mM TMB and 25 mM H_2O_2. The chromogenic reaction was allowed to stand for 2 min, and then, the UV–vis absorption spectrum was recorded in the range of 300–800 nm. The absorption peak located at 652 nm was selected to determine the concentration of the target NOS sequences.

By following the above procedures, the NOS segments in the initial total extracted DNA and PCR products of GM tomato were detected using the fabricated colorimetric biosensor.

3. Results and discussion

3.1. Characterization of Fe_3O_4@Au@cDNA@H-GN nanocomposite

The morphology of the prepared nanomaterials was characterized using SEM or TEM. The synthesized Fe_3O_4 MNPs are cubic in shape, with smooth surface (Fig. 1A and B). The particle size of the Fe_3O_4 MNPs ranges from 125 to 375 nm. After immersed in a PEI solution for 1 h and then in an Au NP solution for another 1 h, the surface of Fe_3O_4 NPs turned from smooth into rough (Fig. 1C). It is obvious that Au NPs (~4 nm, Fig. 1C inset) attach and distribute densely on the surface of Fe_3O_4 NPs. When cDNA was bound covalently with Fe_3O_4@Au through Au–S bonds and then further bound with H-GN though the π interactions between cDNA and H-GN, Fe_3O_4@Au MNPs appeared to be wrapped in H-GN and became ambiguous to observed (Fig. 1D). Furthermore, H-GN in the Fe_3O_4@Au@cDNA@H-GN nanostructure shows a typical flake-like shape with slight wrinkles, which is similar to the morphology of H-GN (Fig. 1D inset). These results suggest the successful preparation of the Fe_3O_4@Au@cDNA@H-GN composite.

The nanomaterials used in the present work were characterized with

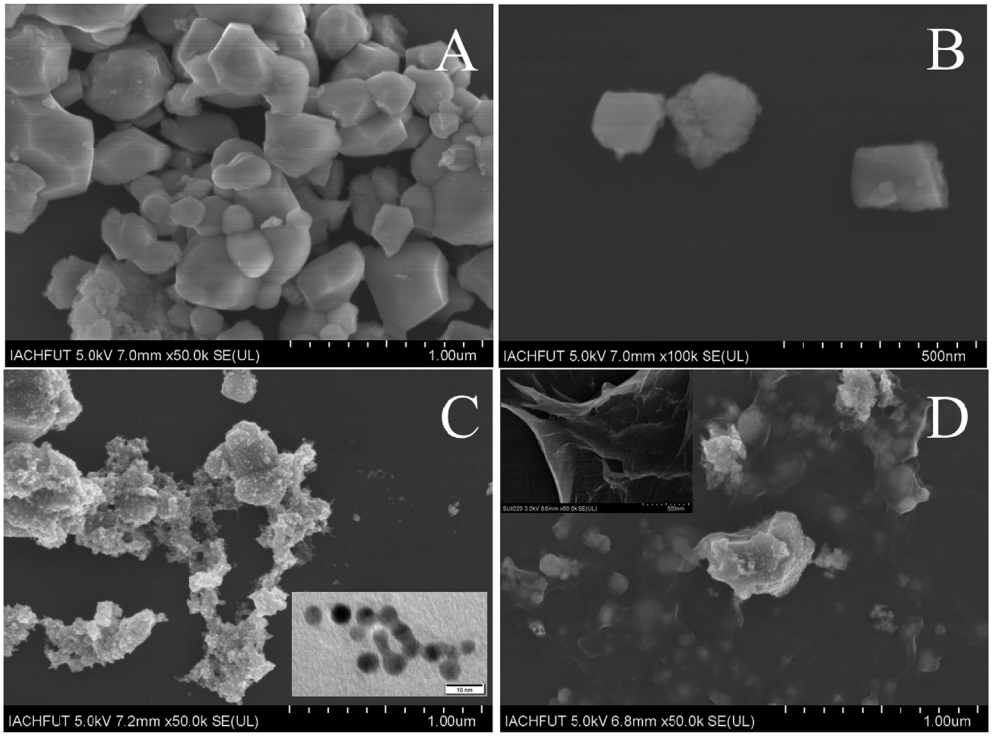

Fig. 1. Morphology characterization of various nanomaterials. SEM images of Fe_3O_4 MNPs (A) with a closer look (B), Fe_3O_4@Au MNPs (C) and Fe_3O_4@Au@cDNA@H-GN nanocomposite (D). The inset of (C) is the TEM image of Au NPs, and the inset of (D) is the SEM image of H-GN.

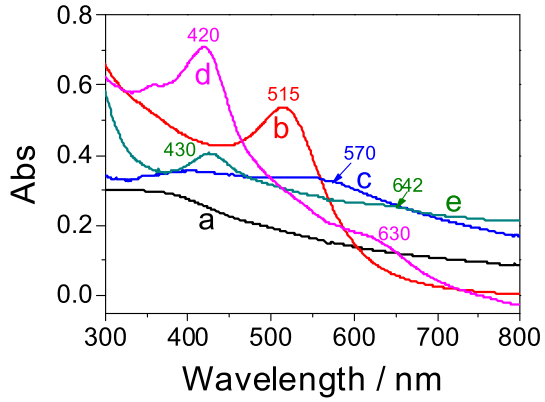

Fig. 2. UV–vis spectra of Fe_3O_4 NP (a), Au NP (b), Fe_3O_4@Au NP (c), H-GN (d) and Fe_3O_4@Au@cDNA@H-GN (e).

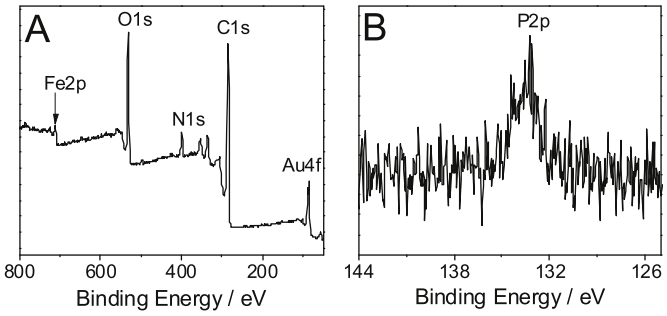

Fig. 3. Survey XPS pattern of Fe_3O_4@Au@cDNA@H-GN nanocomposite (A) and XPS spectrum of P2p in Fe_3O_4@Au@cDNA@H-GN (B).

UV–vis spectroscopy, and the absorbance curves are displayed in Fig. 2. There is a broad absorbance at wavelength between 300 and 500 nm in the spectrum of the PEI-wrapped Fe_3O_4 NPs (Fig. 2 curve a). The absorption might be associated with the *d–d* transition of Fe^{3+} [35]. The maximum absorption of Au NPs is located at 515 nm (Fig. 2 curve b). There are two broad absorption peaks in Fe_3O_4@Au NPs (Fig. 2 curve c), which are related to the UV–vis absorbances of Fe_3O_4 and Au NPs in Fe_3O_4@Au NPs. It is obvious that the absorption peak of Au NPs redshifted to approximately 570 nm. This shift may result from the interaction between Fe_3O_4 and Au NPs or aggregation of Au NPs. The UV–vis absorbance of H-GN from 300 to 800 nm shows a maximum and broad absorption band at 420 nm, along with a shoulder band at ~630 nm (Fig. 2 curve d); these two peaks can be assigned to the Sorët band and Q-band of hemin [31], respectively. After H-GN was bound to the surface of Fe_3O_4@Au NPs via cDNA, these two peaks redshifted to 430 nm and 642 nm, respectively (Fig. 2 curve e). Such shifts are due to the strong interaction between H-GN and Fe_3O_4@Au@cDNA. These results demonstrate the successful preparation of the Fe_3O_4@Au@cDNA@H-GN nanocomposite.

The elemental composition of Fe_3O_4@Au@cDNA@H-GN was then analyzed by XPS. The peaks at 710.96, 532.17, 398.51, 274.82 and 84.26 eV in the survey XPS pattern (Fig. 3A) are assigned to Fe2p, O1s, N1s, C1s and Au4f, respectively. As shown in Fig. 3B, there is a peak with a maximum binding energy at 133.4 eV, which is related to the binding energy of P2p [36], demonstrating the presence of cDNA. These results also indicate the successful preparation of the Fe_3O_4@Au@cDNA@H-GN nanocomposite.

3.2. Strategy and sensing principle for target NOS sequences

The strategy for determination of the target NOS sequences was based on the difference in absorbing ability of H-GN towards ssDNA and dsDNA sequences. As illustrated in Scheme 1, when the hybridization event between cDNA and its complementary DNA (tDNA) sequence happens, H-GN will release from the newly formed nanostructure of Fe_3O_4@Au@cDNA-tDNA due to weaker interaction between H-GN and dsDNA. The quantitative sensing for the target NOS sequences was based on the excellent peroxidase-mimicking activity of H-GN to promote the catalytic oxidation of TMB in presence of H_2O_2. The

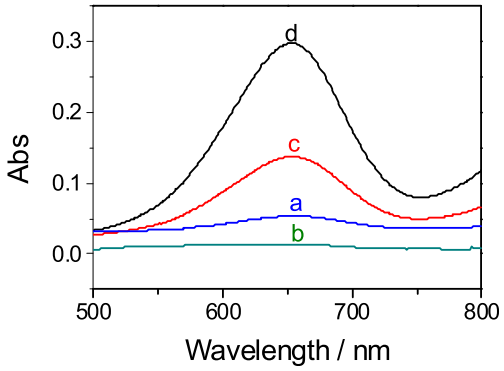

Fig. 4. UV–vis spectra recorded after Fe_3O_4@Au@cDNA@H-GN hybridized with 0 nM (a), 0.5 nM (c) and 10 nM (d) of target NOS sequences. UV–vis spectrum recorded after Fe_3O_4@Au@cDNA@GN hybridized with 10 nM (b) of target NOS sequences. The concentrations of TMB and H_2O_2 were 0.4 and 25 mM, respectively. The pH value of phosphate buffer was 5.0.

colorimetric absorbance intensity at 652 nm depends on the amount of H-GN. The more the H-GN is released, the greater the intensity that the chromogenic system will exhibit. As shown in Fig. 4, the chromogenic system exhibits a slight absorbance at 652 nm in absence of the target NOS sequences (Fig. 4, curve a). However, the absorbance at 652 nm increased significantly after the cDNA in Fe_3O_4@Au@cDNA@H-GN hybridized with 0.5 nM target NOS (Fig. 4, curve c). The intensity was further increased after hybridization with 10 nM target NOS (Fig. 4, curve d). Moreover, it is easy to conclude that H-GN shows better enzymatic activity than GN in the TMB-H_2O_2 chromogenic system (Fig. 4, curve b, c, and d). These results confirm the feasibility of our sensing principle.

3.3. Optimization of experimental parameters

In this study, several experimental parameters were optimized including the concentrations of TMB and H_2O_2, the pH value of the chromogenic reaction solution, the hybridization temperature and the time. To achieve the best analytical performance in detecting target NOS sequences, the colorimetric assay should be conducted under the following conditions: (1) 0.4 mM of TMB (Fig. 5 A); (2) 25 mM of H_2O_2 (Fig. 5 B); (3) pH 5.0 of chromogenic reaction solution (Fig. 5 C); (4) hybridization temperature of 37 °C (Fig. 5 D); and (5) hybridization time of 120 min (Fig. 5 E).

3.4. Analytical performance for detection of target NOS sequences

The analytical performance of the developed colorimetric biosensor was investigated under optimal conditions by using various concentrations of target NOS sequences. As depicted in Fig. 6 A, the peak intensity at 652 nm is strengthened as the target NOS concentration increases, and the color of the chromogenic reaction solutions turns from colorless to blue (Fig. 6 A inset). The relationship between the blank-subtracted peak intensity (ΔAbs) and the concentration of the target NOS is shown in Fig. 6 B. The ΔAbs values show good linearity with the logarithm of the target NOS concentration in the range of 0.5–200 nM (Fig. 6 B, inset). The linear regression equation is written as $\Delta Abs = 0.173\ \lg C\ (M) + 1.706$, with a correlation coefficient (R) of 0.995 and a detection limit of 0.19 nM. The detection limit is lower than that of the reported "signal-off" colorimetric assay for specific DNA sequence using H-GN only as the peroxidase mimic [28]. This result may be due to the reduced blank signal in the current biosensing by the use of Fe_3O_4@Au. The analytical performance of our biosensor was also compared with that of other GMO biosensors, and the results are listed in Table 1. As seen from the table, the presented colorimetric assay displays a comparable [17] or low detection limit than that of most GMO biosensors [37–39]. In addition, the analytical performance in the linear range of our biosensor is comparable to that of the colorimetric biosensor using DNA-based materials [17] and fluorescence biosensors [38], and the linear range obtained for this colorimetric biosensor is wider than that of the other reported biosensors [37,39]. These results demonstrate the present method has potential for GM content monitoring.

3.5. Selectivity and stability

The specificity of the promoted biosensor was investigated before its application in real samples. The experiment was performed by challenging the sensing system with other DNA sequences including the CaMV35S gene sequence, single-base mismatched (Mis1), double-based mismatched (Mis2) and three-base mismatched (Mis3) DNA sequences. The sensing system showed the strongest response towards the target NOS sequences among the DNA sequences (Fig. 7A). The system showed an absorbance of 0.21 to Mis1 (1 mM), which was 41.2% that with the target NOS (100 nM). However, when the concentration of Mis1 was the same as that of the target NOS, the sensing system showed an absorbance of 0.07. This result shows that Mis1 at low concentration has little interference to the detection of the target NOS. The results indicate an acceptable selectivity in detecting target NOS. The storage stability of the prepared Fe_3O_4@Au@cDNA@H-GN was investigated by using the nanocomposite (stored in refrigerator at 4 °C with 1–16 days) to detect 1 nM target NOS. The absorbance intensity is displayed in Fig. 7 B. As seen from the figure, the intensity shows little change after 16 days storage. The result indicates the good storage stability of the prepared Fe_3O_4@Au@cDNA@H-GN nanocomposite.

3.6. Detection of NOS sequence in real samples

The feasibility of practical application of the present biosensor was evaluated by measuring the target NOS in the extracted DNA in GM plants. The PCR products from GM tomato leaves were analyzed by agarose gel electrophoresis. As shown in Fig. 8 A, the PCR products of the target NOS appears at 250 bp (lane 4). No band at this position can be found in non-GM tomato (lane 2), initial total extracted DNA of GM tomato (lane 3), and NOS PCR products of GM tomato without primers (lane 5). This analysis indicates the existence of target NOS sequences in GM tomato. The target NOS sequences in these solutions were detected with the presented method, and the signals are displayed in Fig. 8 B. By comparing the blank control (curve a), no obvious signal can be found for detecting the PCR products of non-GM tomato (curve b, corresponding to lane 2 in Fig. 8 A). This result demonstrates that there are no target NOS segments in non-GM tomato. Strong signals can be observed when detecting the solutions of the PCR products of GM tomato without primers (curve c, corresponding to lane 5 in Fig. 8 A), the initial total extracted DNA (curve d, corresponding to lane 3 in Fig. 8 A), and the PCR products of GM tomato (curve e, corresponding to lane 4 in Fig. 8 A). The biosensor gave the strongest signal in detecting the PCR products of GM tomato. These results demonstrate the feasibility of our fabricated biosensor in the detection of the target NOS in real GM samples. More importantly, this biosensor can be used in the detection of NOS in samples without PCR amplification, suggesting a potential method for discriminating GM and non-GM plants. The reliability of the proposed method was verified by using the standard addition method. The amount of target NOS in an unknown sample prepared with the PCR products was 0.436 nM. When adding the standard solution with concentrations of 5 nM and 10 nM, good recoveries of 93.6 ± 3.0% and 94.2 ± 3.9% (n = 3) were obtained, respectively. This result indicates good reliability of our proposed method.

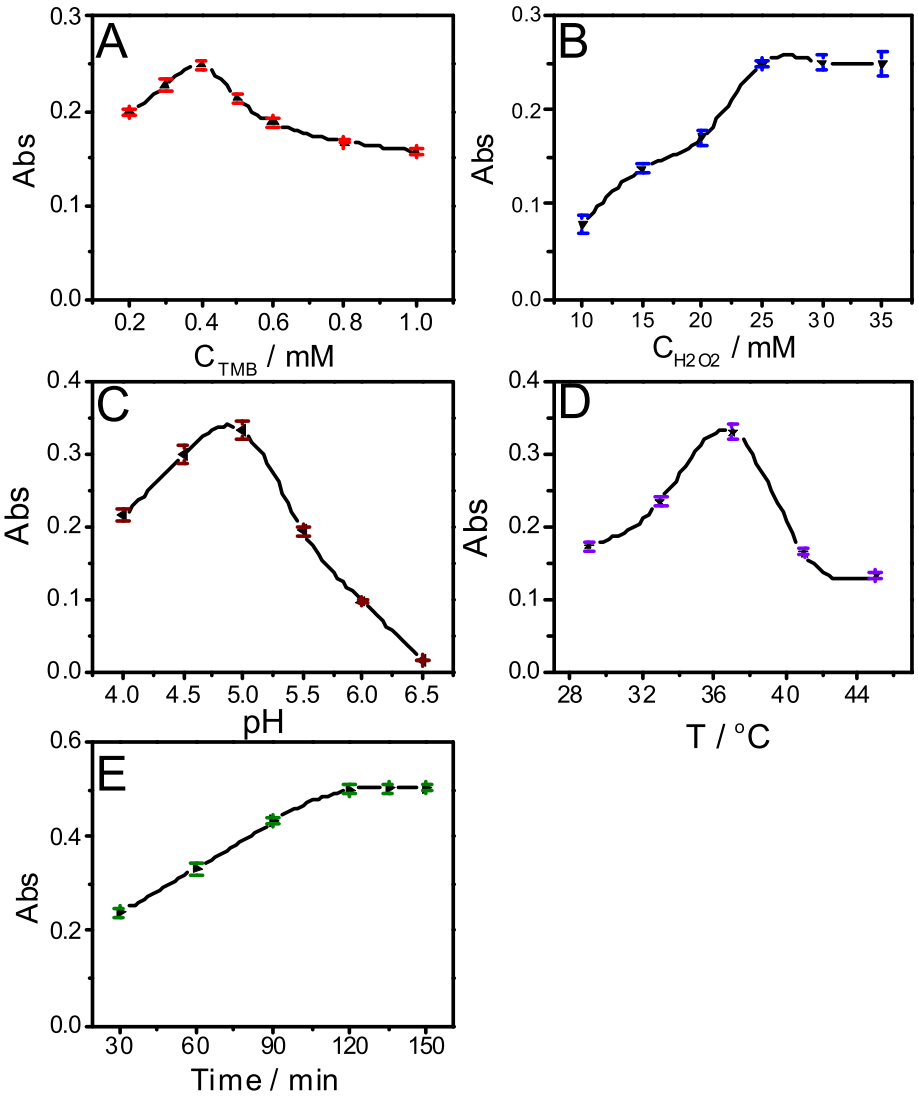

Fig. 5. Effect of the concentrations of TMB (A) and H_2O_2 (B), the pH value of chromogenic reaction solution (C), the hybridization temperature (D) and time (E) on the performance of the colorimetric assay. The concentration of tDNA was 100 nM.

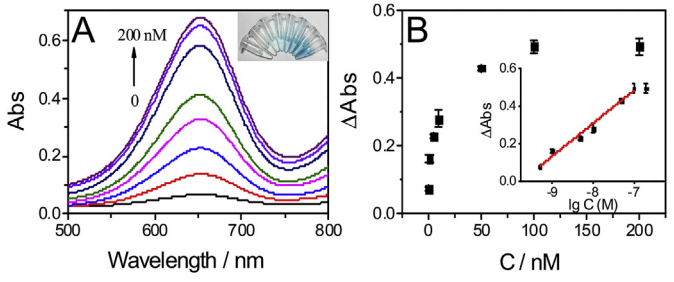

Fig. 6. UV–vis absorption spectra related to the detection of various concentrations of target NOS. From bottom to top are the UV–vis curves of detecting 0, 0.5, 1, 5, 10, 50, 100 and 200 nM target NOS. Inset is the photographs of the corresponding chromogenic reaction solutions. (B) The relationship between the blank subtracted peak intensity at 652 nm and the tDNA concentration. Inset shows the linear relationship between the blank subtracted absorption intensity and the logarithm of tDNA concentration.

4. Conclusions

In summary, we developed a simple and label-free colorimetric biosensor for the detection of NOS gene sequences in GM plant. The cDNA was used as a bridge to link Fe_3O_4@Au NP and H-GN to form the Fe_3O_4@Au@cDNA@H-GN nanocomposite. In the presence of the target NOS, some of the linked H-GN was forced to be released from the surface of Fe_3O_4@Au@cDNA due to the weak affinity between dsDNA and H-GN when the hybridization event between cDNA and target NOS happened. By taking advantages of magnetic separation of Fe_3O_4 and peroxidase-like activity of H-GN towards TMB in the presence of H_2O_2, the constructed "signal-on" biosensor gives a broad linear range and a low detection limit of 0.19 nM. The biosensor shows not only good analytical performance in terms of selectivity and stability but also feasibility in detecting NOS in GM tomato, suggesting a potential method for practical use in identifying GM plants.

Funding

The project is supported by the National Natural Science Foundation of China (Grant Nos. 31772099, 31401573 and 21505071), the Natural Science Foundation of Anhui Province (No. 1908085MC98), the Anhui Key Research and Development Program (Nos. 201904a06020030, 201903b06020007), and the China Postdoctoral Science Foundation (Grant Nos. 2016M592050, 2017T100446).

Table 1
Comparison in the analytical performance between the current biosensor and other nucleotide-based biosensors in detection of GM content.

Nanomaterials for fabricated biosensors	DNA-based materials	Methods	Target	Detection limit	Linear range	Ref.
–	Hemin/G-quadruplex DNAzyme	Colorimetry	CaMV35S	0.23 nM	0.5–500 nM	[17]
–	Hemin/G-quadruplex DNAzyme	Colorimetry	CaMV35S	5 nM	50–500 nM	[37]
Multiwalled carbon nanotubes@graphene oxide nanoribbons	CdTe quantum dots-labeled probe	Fluorescence	NOS	0.5 nM	1.5–1000 nM	[38]
			CaMV35S	0.35 nM	1.2–900 nM	
Streptavidin-coated magnetic beads	Biotin-probe and ruthenium (II) tris-bipyridal-probe	Electrochemiluminescence	CaMV35S	5 nM	5–500 nM	[39]
Fe_3O_4@Au@cDNA@H-GN nanocomposite	–	Colorimetry	NOS	0.19 nM	0.5–100 nM	This work

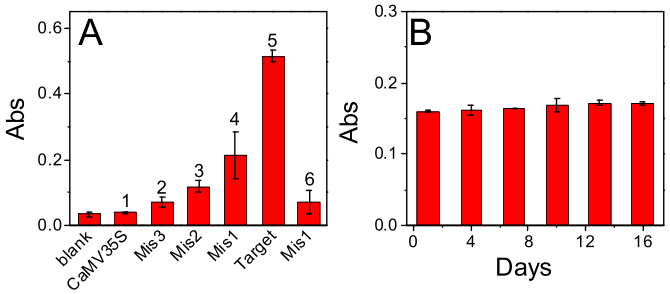

Fig. 7. (A) Specificity of the promoted biosensor for target NOS against other DNA sequences. Columns from 1 to 4 are other sequences, each with concentration of 1 mM. Column 5 and 6 are the obtained responses on the biosensor to the target NOS (100 nM) and Mis 1 (100 nM), respectively. (B) Storage stability of Fe_3O_4@Au@cDNA@H-GN. The concentration of target NOS was 1 nM.

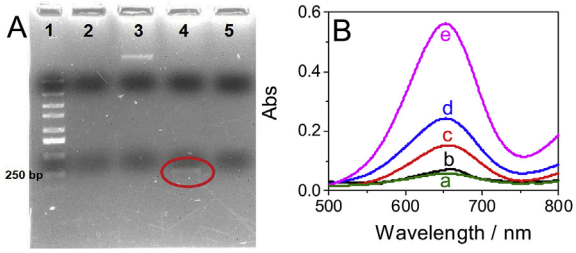

Fig. 8. (A) Inverse image of agarose gel electrophoresis for marker (lane 1), NOS PCR products from non-GM tomato (lane 2), initial total extracted DNA of GM tomato without template and primer (lane 3), NOS PCR products of GM tomato (lane 4) and NOS PCR products of GM tomato without primers (lane 5). (B) Colorimetric detection for various samples: blank control (a), PCR products of non-GM tomato (b, corresponding to lane 2), PCR products of GM tomato without primers (c, corresponding to lane 5), initial total extracted DNA of GM tomato (d, corresponding to lane 3) and PCR products of GM tomato (e, corresponding to lane 4).

Authors' contributions

Xiaodong Cao and Yongkang Ye: Conceptualization; Xiaodong Cao Yongkang Ye and Zihao Xia: Methodology; Xiaodong Cao and Zihao Xia: Writing—original draft preparation; Wuwen Yan: Assistance in data processing; Xuan Xu, Shudong He, Zhaojun Wei and Haisong Zheng: Writing—review and editing; Xiaodong Cao and Yongkang Ye; Supervision; Yongkang Ye, Xiaodong Cao, Xuan Xu and Haisong Zheng: Funding acquisition.

References

[1] C. James, Biotech crops continue to help meet the challenges of increased population and climate change, ISAAA Briefs 54 (2018) 324 https://www.isaaa.org/resources/publications/briefs/54/executivesummary/default.asp.
[2] J. Song, B. Niu, D. Wang, F. Zhang, Quantifying the measurement uncertainty of the nopaline synthase terminator in mixed samples of genetically modified rice using a bottom-up approach, Food Contr. 73 (2017) 1548–1555, https://doi.org/10.1016/j.foodcont.2016.11.020.
[3] M. Singh, G.J. Randhawa, P. Sood, R.K. Bhoge, Loop-mediated isothermal amplification targeting insect resistant and herbicide tolerant transgenes: monitoring for GM contamination in supply chain, Food Contr. 51 (2015) 283–292, https://doi.org/10.1016/j.foodcont.2014.11.045.
[4] R. Li, J. Shi, B. Liu, C. Wang, D. Zhang, X. Zhao, L. Yang, Inter-laboratory validation of visual loop-mediated isothermal amplification assays for GM contents screening, Food Chem. 274 (2019) 659–663, https://doi.org/10.1016/j.foodchem.2018.07.010.
[5] W. Gao, J. Tian, K. Huang, Z. Yang, W. Xu, Y. Luo, Ultrafast, universal and visual screening of dual genetically modified elements based on dual super PCR and a lateral flow biosensor, Food Chem. 279 (2019) 246–251, https://doi.org/10.1016/j.foodchem.2018.12.013.
[6] S.-H. Jung, H. Jang, M.-C. Lim, J.-H. Kim, K.-S. Shin, S.M. Kim, H.-Y. Kim, Y.-R. Kim, T.-J. Jeon, Chromatic biosensor for detection of phosphinothricin acetyltransferase by use of polydiacetylene vesicles encapsulated within automatically generated immunohydrogel beads, Anal. Chem. 87 (2015) 2072–2078, https://doi.org/10.1021/ac501795x.
[7] J.B. Sousa, J. Ramos-Jesus, L.C. Silva, C. Pereira, N. de-los-Santos-Álvarez, R.A.S. Fonseca, R. Miranda-Castro, C. Delerue-Matos, J.R. Santos, M.F. Barroso, Fe_3O_4@Au nanoparticles-based magnetoplatform for the HMGA maize endogenous gene electrochemical genosensing, Talanta 206 (2020) 120220, https://doi.org/10.1016/j.talanta.2019.120220.
[8] Y. Ye, S. Mao, S. He, X. Xu, X. Cao, Z. Wei, S. Gunasekaran, Ultrasensitive electrochemical genosensor for detection of CaMV35S gene with Fe_3O_4-Au@Ag nanoprobe, Talanta 206 (2020) 120205, https://doi.org/10.1016/j.talanta.2019.120205.
[9] C. Qian, R. Wang, H. Wu, J. Ping, J. Wu, Recent advances in emerging DNA-based methods for genetically modified organisms (GMOs) rapid detection, Trac. Trends Anal. Chem. 109 (2018) 19–31, https://doi.org/10.1016/j.trac.2018.09.021.
[10] S. Wei, C. Wang, P. Zhu, G. Zhou, W. Fu, X. Wu, A high-throughput multiplex tandem PCR assay for the screening of genetically modified maize, LWT - Food Sci. Technol. (Lebensmittel-Wissenschaft -Technol.) 87 (2018) 169–176, https://doi.org/10.1016/j.lwt.2017.08.061.
[11] P. Safaei, E.M. Aghaee, G.J. Khaniki, S.A.K. Afshari, S. Rezaie, A simple and accurate PCR method for detection of genetically modified rice, J. Environ. Health Sci. 17 (2019) 847–851, https://doi.org/10.1007/s40201-019-00401-x.
[12] N. Datukishvili, T. Kutateladze, I. Gabriadze, K. Bitskinashvili, B. Vishnepolsky, New multiplex PCR methods for rapid screening of genetically modified organisms, Foods Front. Microbiol. 6 (2015) 757, https://doi.org/10.3389/fmicb.2015.00757.
[13] Y.J. Li, T. Xiong, H.W. Wu, Y.Z. Yang, Visual DNA microarray coupled with multiplex-PCR for the rapid detection of twelve genetically modified maize, BioChip J. 10 (2016) 42–47, https://doi.org/10.1007/s13206-016-0106-y.
[14] M.L. Ha, N.Y. Lee, Miniaturized polymerase chain reaction device for rapid identification of genetically modified organisms, Food Contr. 57 (2015) 238–245, https://doi.org/10.1016/j.foodcont.2015.04.014.
[15] D. Kayğusuz, S. Vural, A.Ö. Aytekin, S.J. Lucas, M. Elitas, DaimonDNA: a portable, low-cost loop-mediated isothermal amplification platform for naked-eye detection of genetically modified organisms in resource-limited settings, Biosens. Bioelectron. 141 (2019) 111409, https://doi.org/10.1016/j.bios.2019.111409.
[16] C. Wang, N. Cheng, L. Zhu, Y. Xu, K. Huang, P. Zhu, S. Zhu, W. Fu, W. Xu, Colorimetric biosensor based on a DNAzyme primer and its application in logic gate operations for DNA screening, Anal. Chim. Acta 987 (2017) 111–117, https://doi.org/10.1016/j.aca.2017.08.001.
[17] D. Zhang, W. Wang, Q. Dong, Y. Huang, D. Wen, Y. Mu, Y. Yuan, Colorimetric detection of genetically modified organisms based on exonuclease III-assisted target recycling and hemin/G-quadruplex DNAzyme amplification, Microchim. Acta 185 (2018) 75, https://doi.org/10.1007/s00604-017-2618-0.
[18] E. Nourisaeid, A. Mousavi, A. Arpanaei, Colorimetric DNA detection of transgenic plants using gold nanoparticles functionalized with L-shaped DNA probes, Phys. E 75 (2016) 188–195, https://doi.org/10.1016/j.physe.2015.09.018.
[19] X. Wang, Z. Fu, X. Chen, C. Peng, X. Xu, W. Wei, F. Li, J. Xu, Use of a novel metal indicator to judge loop-mediated isothermal amplification for detecting the 35S promoter, Anal. Bioanal. Chem. 409 (2017) 881–889, https://doi.org/10.1007/s00216-016-0084-x.
[20] M. Singh, R.K. Bhoge, G. Randhawa, Real-time and visual loop-mediated isothermal amplification: efficient GMO screening targeting *pat* and *pmi* marker genes, Food Contr. 71 (2017) 248–254, https://doi.org/10.1016/j.foodcont.2016.06.027.
[21] H.A. Kermani, M. Hosseini, A. Miti, M. Dadmehr, G. Zuccheri, S. Hosseinkhani, M.R. Ganjali, A colorimetric assay of DNA methyltransferase activity based on

peroxidase mimicking of DNA template Ag/Pt bimetallic nanoclusters, Anal. Bioanal. Chem. 410 (2018) 4943–4952, https://doi.org/10.1007/s00216-018-1143-2.
[22] Y.S. Borghei, M. Hosseini, M.R. Ganjali, Oxidase-like Catalytic activity of Cys-AuNCs upon visible light irradiation and its application for visual miRNA detection, Sensor. Actuator. B Chem. 273 (2018) 1618–1626, https://doi.org/10.1016/j.snb.2018.07.061.
[23] C. Wang, D. Chen, Q. Wang, R. Tan, Kanamycin detection based on the catalytic ability enhancement of gold nanoparticles, Biosens. Bioelectron. 91 (2017) 262–267, https://doi.org/10.1016/j.bios.2016.12.042.
[24] L. Huang, K. Chen, W. Zhang, X. Zhu, J. Wang, R. Wang, N. Hu, Y. Suo, J. Wang, ssDNA-tailorable oxidase-mimicking activity of spinel $MnCo_2O_4$ for sensitive biomolecular detection in food sample, Sensor. Actuator. B Chem. 269 (2018) 79–87, https://doi.org/10.1016/j.snb.2018.04.150.
[25] C. Lu, X. Liu, Y. Li, F. Yu, L. Tang, Y. Hu, Y. Ying, Multifunctional Janus hematite−silica nanoparticles: mimicking peroxidase-like activity and sensitive colorimetric detection of glucose, ACS Appl. Mater. Interfaces 7 (2015), https://doi.org/10.1021/acsami.5b03423 15395−15402.
[26] Y. Fan, W. Zhang, Y. Liu, Z. Zeng, X. Quan, H. Zhao, Three-dimensional branched crystal carbon nitride with enhanced intrinsic peroxidase-like activity: a hypersensitive platform for colorimetric detection, ACS Appl. Mater. Interfaces 11 (2019) 17467–17474, https://doi.org/10.1021/acsami.9b04320.
[27] C. Chen, N. Li, J. Lan, X. Ji, Z. He, A label-free colorimetric platform for DNA via target-catalyzed hairpin assembly and the peroxidase-like catalytic of graphene/Au-NPs hybrids, Anal. Chim. Acta 902 (2016) 154–159, https://doi.org/10.1016/j.aca.2015.10.030.
[28] Y. Tao, Y. Lin, J. Ren, X. Xu, Self-assembled, functionalized graphene and DNA as a universal platform for colorimetric assays, Biomaterials 34 (2013) 4810–4817, https://doi.org/10.1016/j.biomaterials.2013.03.039.
[29] C. Wang, J. Qian, K. Wang, X. Yang, Q. Liu, N. Hao, C. Wang, X. Dong, X. Huang, Colorimetric aptasensing of ochratoxin A using Au@Fe_3O_4 nanoparticles as signal indicator and magnetic separator, Biosens. Bioelectron. 77 (2016) 1183–1191, https://doi.org/10.1016/j.bios.2015.11.004.
[30] M. Ma, J. Xie, Y. Zhang, Z. Chen, N. Gu, Fe_3O_4@Pt nanoparticles with enhanced peroxidase-like catalytic activity, Mater. Lett. 105 (2013) 36–39, https://doi.org/10.1016/j.matlet.2013.04.020.
[31] Y. Ye, J. Gao, H. Zhuang, H. Zheng, H. Sun, Y. Ye, X. Xu, X. Cao, Electrochemical gene sensor based on a glassy carbon electrode modified with hemin-functionalized reduced graphene oxide and gold nanoparticle-immobilized probe DNA, Microchim. Acta 184 (2017) 245–252, https://doi.org/10.1007/s00604-016-1999-9.
[32] X. Wei, Y. Wang, J. Chen, P. Xu, W. Xu, R. Ni, J. Meng, Y. Zhou, Poly(deep eutectic solvent)-functionalized magnetic metal-organic framework composites coupled with solid-phase extraction for the selective separation of cationic dyes, Anal. Chim. Acta 1056 (2019) 47–61, https://doi.org/10.1016/j.aca.2018.12.049.
[33] K.C. Grabar, K.J. Allison, B.E. Baker, R.M. Bright, K.R. Brown, R.G. Freeman, A.P. Fox, C.D. Keating, M.D. Musick, M.J. Natan, Two-dimensional arrays of colloidal gold particles: a flexible approach to macroscopic metal surfaces, Langmuir 12 (1996) 2353–2361, https://doi.org/10.1021/la950561h.
[34] X. Wang, D. Teng, F. Tian, Q. Guan, J. Wang, Comparison of three DNA extraction methods for feed products and four amplification methods for the 5′-junction fragment of Roundup Ready Soybean, J. Agric. Food Chem. 60 (2012) 4586–4595, https://doi.org/10.1021/jf300827q.
[35] D.A. Skoog, F.J. Holler, T.A. Nieman, Principle of Instrumental Analysis, fifth ed., Harcourt Brace & Company, USA, 1998, pp. 336–340.
[36] Z.-C. Liu, X. Zhang, N.-Y. He, Z.-H. Lu, Z.-C. Chen, Probing DNA hybridization efficiency and single base mismatch by X-ray photoelectron spectroscopy, Colloids Surf., B 71 (2009) 238–242, https://doi.org/10.1016/j.colsurfb.2009.02.013.
[37] X. Jiang, H. Zhang, J. Wu, X. Yang, J. Shao, Y. Lu, B. Qiu, Z. Lin, G. Chen, G-quadruplex DNA biosensor for sensitive visible detection of genetically modified food, Talanta 128 (2014) 445–449, https://doi.org/10.1016/j.talanta.2014.05.002.
[38] Y. Li, L. Sun, J. Qian, L. Long, H. Li, Q. Liu, J. Cai, K. Wang, Fluorescent “on-off-on” switching sensor based on CdTe quantum dots coupled with multiwalled carbon nanotubes@graphene oxide nanoribbons for simultaneous monitoring of dual foreign DNAs in transgenic soybean, Biosens. Bioelectron. 92 (2017) 26–32, https://doi.org/10.1016/j.bios.2017.01.057.
[39] D. Zhu, J. Liu, Y. Tang, D. Xing, A reusable DNA biosensor for the detection of genetically modified organism using magnetic bead-based electrochemiluminescence, Sensor. Actuator. B Chem. 149 (2010) 221–225 http://doi:10.1016/j.snb.2010.05.047.